Structural characterization and hydrogen storage properties of the Ti31V26Nb26Zr12M5 (M = Fe, Co, or Ni) multi-phase multicomponent alloys

Lucas Faccioni Chanchetti, Bruno Hessel Silva, Jorge Montero, Claudia Zlotea, Yannick Champion, Walter José Botta, Guilherme Zepon

Structural characterization and hydrogen storage properties of the $Ti_{31}V_{26}Nb_{26}Zr_{12}M_5$ (M = Fe, Co, or Ni) multi-phase multicomponent alloys

Lucas Faccioni Chanchetti[a], Bruno Hessel Silva[b], Jorge Montero[c], Claudia Zlotea[c], Yannick Champion[d], Walter José Botta[a,b], Guilherme Zepon[a,b,#]

a - Federal University of São Carlos, Department of Materials Engineering (DEMa/UFSCar) - Rodovia Washington Luiz, km 235, São Carlos – São Paulo, Brazil CEP:13565-905.

b - Federal University of São Carlos, Graduate Program in Materials Science and Engineering, (PPGCEM/UFSCar) - Rodovia Washington Luiz, km 235, São Carlos – São Paulo, Brazil CEP:13565-905.

c - Univ Paris Est Créteil, CNRS, ICMPE, UMR 7182, 2 Rue Henri Dunant, 94320, Thiais, France.

d - Univ. Grenoble Alpes, CNRS, G-INP, SIMaP, 38000 Grenoble, France.

 # Corresponding author: zepon@ufscar.br

Abstract

Structure and hydrogen storage properties of three $Ti_{31}V_{26}Nb_{26}Zr_{12}M_5$ multicomponent alloys with M = Fe, Co and Ni are investigated. The alloys synthesized by arc melting are characterized via X-Ray Diffraction (XRD) and Scanning Electron Microscopy (SEM). The as-cast ingots present multi-phase dendritic structures composed mainly of BCC phases and small amounts of C14 Laves phases. Upon hydrogenation, each alloy absorbs around 1.9 H/M (number of hydrogen atoms per metal atoms) at room temperature. XRD of fully hydrogenated samples shows the formation of multi-phase structures composed of FCC and C14 hydrides. Thermo Desorption Spectroscopy (TDS) shows that the hydrogenated alloys present multi-step desorption processes with wide temperature ranges and low onset temperatures. XRD of partially hydrogenated samples indicate the presence of intermediate BCC hydrides. XRD of desorbed samples suggest reversible reactions of absorption/desorption: BCC + C14 alloy ↔ intermediate BCC hydride + C14 hydride ↔ FCC + C14 hydrides.

Keywords: Multi-phase multicomponent alloys, hydrogen storage, hydrogen desorption

1. Introduction

The current use of hydrogen in the energy sector is largely confined to oil refining and production of ammonia/methanol [1,2]. The obtention of hydrogen by water electrolysis via renewable energy sources and its application as an energy carrier has been discussed as an option to expand the use of hydrogen [1,3]. The high calorific energy and the potential to achieve net-zero CO_2 emissions in many sectors are examples of the benefits from a hydrogen based energy matrix [1,4]. However, hydrogen storage is considerably challenging due to its flammability and low volumetric densities at room temperature [5]. Presently, the main options to store hydrogen are based on 1) physical storage technologies such as high pressure cylinders and cryogenic liquid storage and 2) material storage technologies such as in complex hydrides, hydrogen adsorbents materials and metal hydrides [6,7]. Metal hydrides are often discussed as a method to store hydrogen in the solid-state with high volumetric efficiency and to diminish risks related to safety concerns such as leakages or explosions [8,9]. However, most conventional metal hydrides present limitations such as low gravimetric storage capacity, sluggish kinetics of absorption/desorption, poor cycling stability and/or undesirable thermodynamic behavior [5,10].

Recently, novel alloys generically know as multicomponent alloys have been proposed as candidates for hydrogen storage applications. These alloys present at least 3 elements with substantial atomic fraction in their chemical composition exploring the center area of multicomponent phase diagrams [11]. The majority of H_2-related studies on this subject have been investigating two types of multicomponent alloys, body centered cubic (BCC) alloys and the intermetallic Laves C14 alloys [10–29]. BCC alloys generally present absorption levels around 2 H/M and form dihydrides with face centered cubic (FCC) structure, or body centered tetragonal (BCT) structure [11,16,24,31]. On the other hand, intermetallic Laves C14 alloys usually absorb 1 H/M forming monohydrides maintaining the C14 structure type with expanded lattice parameters [11,12,23]. Studies on hydrogen storage properties in multi-phase multicomponent alloys have also been reported [32,33]. Recently, Sleiman et al. [32] studied the microstructure and hydrogen storage properties of the multi-phase $Ti_{0.3}V_{0.3}Mn_{0.2}Fe_{0.1}Ni_{0.1}$ alloy. The authors reported the alloy presented a microstructure mainly composed of C14 Laves phase with a minor amount of BCC phase (around 10%). They also reported that the alloy absorbed 1.6 wt.% of hydrogen within an hour at room temperature without the need of a prior heat treatment to facilitate hydrogen absorption. XRD analyses suggested that both BCC and Laves phase absorbed hydrogen maintaining their crystal structure and increasing their lattice parameters. These works evidenced

the variety and complexity of the possible microstructures in multicomponent alloys and their effect on hydrogen storage. However, the understanding of hydrogen storage mechanisms and properties in these alloys are still in the early stages. Particularly, multi-phase multicomponent alloys have been scarcely analyzed.

Besides the complexity of phase constitutions, the various systems and wide range of chemical compositions allows the combination of elements with different properties/characteristics in multicomponent alloys [11,34]. Therefore, specific properties might be potentially optimized via chemical compositional tuning. For example, in order to obtain lightweight multicomponent alloys for hydrogen storage, researchers have been investigating hydrogen sorption properties of BCC alloys combining transition metal elements such as Ti, V and Zr with lightweight elements such as Mg and Al [20,28,35]. Montero et al. [28] showed that adding Mg in the $Ti_{0.325}V_{0.275}Zr_{0.125}Nb_{0.275}$ multicomponent alloy not only reduced the alloy density but also improved its cycling behavior. The $Mg_{0.10}Ti_{0.3}0V_{0.25}Zr_{0.10}Nb_{0.25}$ alloy presented a stable reversible storage capacity of 2.4 H wt% after 2 cycles of absorption/desorption whereas the base alloy without Mg presented a reversible storage capacity of 1.9 H wt.% after 4 cycles of absorption/desorption. Tuning hydrogen storage properties by combining elements with different hydrogen affinity has been another strategy frequently reported for multicomponent alloys [16,18,19]. For example, Strozi et al. [18] showed that increasing the Cr (non hydride forming element) content in $(TiVNb)_{100-x}Cr_x$ alloys increased the hydrogen equilibrium pressure at room temperature. The authors showed that changing the amount of Cr from 15 to 35 at.% resulted in a shift of the hydrogen equilibrium plateau pressure from 0.01 bar to approximately 2 bar.

In the context of the present work, studies developed by Montero et al. [29,36] brought attention to the hydrogen sorption properties of the $Ti_{0.325}V_{0.275}Nb_{0.275}Zr_{0.125}$ alloy. According to the authors, this single-phase BCC alloy absorbs hydrogen in a single step forming a FCC dihydride with maximum hydrogen uptake around 1.7-1.8 H/M. However, the temperature conditions required to desorb the hydrogenated samples of this alloy were considerably high. Measurements of TDS showed that the maximum desorption rates under secondary vacuum (10^{-6} mbar) were between 200-350 ºC. We believe that the hydrogen affinity of the 4 elements (Ti, V, Nb and Zr) in the alloy determined the high thermodynamic hydride stability and therefore prevented the desorption process to occur at moderate temperatures and pressure conditions. Thus,

in the present work we used the strategy of adding 5 at.% of elements with low hydrogen affinity (Fe, Co and Ni) into the quaternary $Ti_{0.325}V_{0.275}Nb_{0.275}Zr_{0.125}$ alloy. The aim is to investigate the structure and hydrogen storage properties of new $Ti_{31}V_{26}Nb_{26}Zr_{12}M_5$ multicomponent alloys and to compare with the quaternary pristine composition.

2. Materials and methods

2.1. Alloys Synthesis and structural characterization

The three alloys were synthesized by electric arc melting under argon atmosphere using pieces of Ti, V, Nb, Zr, Fe Co and Ni with purity level higher than (99.5 %). The mass of the elements used to produce each alloy are displayed in Table 1. Prior to each alloy synthesis, Ti getter pieces were melted to minimize the oxygen content in the ingots. Each ingot was re-melted at least 3 times to improve chemical homogeneity. The alloys were stored in a Mbraun glovebox under argon atmosphere with levels of O_2 and H_2O lower than 0.5 ppm. The alloys were cut in the cross-section area using a diamond disk to perform structural characterization of the as-cast samples. Subsequently, the piece was embedded in conductive resin, ground with increasingly finer SiC paper and polished with diamond suspensions. The structural characterization performed in this work included XRD, SEM and Energy Dispersive Spectroscopy (EDS) analyses. XRD patterns were acquired in a Panalytical® Xpert Pro MPD and in a D8 Advance Brucker diffractometer, both using Cu-Kα radiation ($\lambda_{K\alpha1}$ = 1.5406 Å, $\lambda_{K\alpha2}$ = 1.5444 Å). Phase identification and Rietveld refinements were performed using the software General Structure Analysis System II (GSAS-II) [37]. SEM and EDS analyses were caried out in a FEG JEOL IT500HR microscope, with an SDD detector from Bruker.

Table 1: Mass amounts of the pure elements used to produce the alloys.

Composition (at.%)	**Ti** (g)	**V** (g)	**Nb** (g)	**Zr** (g)	**Fe** (g)	**Co** (g)	**Ni** (g)
$Ti_{31}V_{26}Nb_{26}Zr_{12}Fe_5$	0.9046(1)	0.8034(1)	1.4655(1)	0.6612(1)	0.1762(1)	-------	-------
$Ti_{31}V_{26}Nb_{26}Zr_{12}Co_5$	1.0496(1)	0.9257(1)	1.7022(1)	0.7740(1)	-------	0.2168(1)	-------
$Ti_{31}V_{26}Nb_{26}Zr_{12}Ni_5$	1.0465(1)	0.9271(1)	1.7073(1)	0.7694(1)	-------	-------	0.2018(1)

2.2. Hydrogen absorption/desorption analyses

For hydrogenation tests, the ingots were cut in small pieces (using a shear manual cutter) and loaded in the Sieverts apparatus. An activation treatment was conducted by heating the samples at 350 °C under dynamic vacuum (10^{-3} mbar) for three hours and cooled them to room temperature prior to hydrogen absorption tests. Hydrogen absorption kinetics were measured at room temperature with H_2 pressures around 42-43 bar. Hydrogen desorption behavior was investigated by TDS analyses, as described in [29]. The samples were heated from room temperature to 450 °C with a temperature ramp of 2 °C/min under secondary vacuum (10^{-6} mbar) in a homemade apparatus. A Quadrupole Mass Spectrometer (MKS MicroVision Plus RGA) recorded the partial H_2 pressure while the temperatures were recorded with a type K thermocouple in direct contact with the powder samples. Partially hydrogenated samples were obtained by subjecting samples to a complete cycle of absorption/desorption followed by a second step of absorption applying the desired amount of hydrogen. The levels of absorption in the partially hydrogenated samples were between 1-1.25 H/M.

3. Results and Discussions

3.1. Structural characterization of the synthesized alloys

Figure 1 shows the XRD patterns of the as-cast samples from $Ti_{31}V_{26}Nb_{26}Zr_{12}M_5$ (M=Fe, Co or Ni) alloys. The three alloys presented multi-phase structures predominantly composed of BCC phases with small amounts of C14 Laves phases. Lattice parameters and phase concentrations determined by Rietveld refinement analyses are listed on Table 2. The Rietveld refinement plots related to these experiments are available in Figure S1 of the supplementary file. Despite some small deviations, the values of phase concentrations and lattice parameters from the BCC and C14 phases were considerably similar among the alloys. It is worth mentioning that these alloys presented BCC phases with lattice parameters slightly reduced in comparison to the base alloy reported by Montero et al. [29] This was expected given that Fe, Co and Ni have smaller atomic radius than Ti, V, Nb and Zr [38].

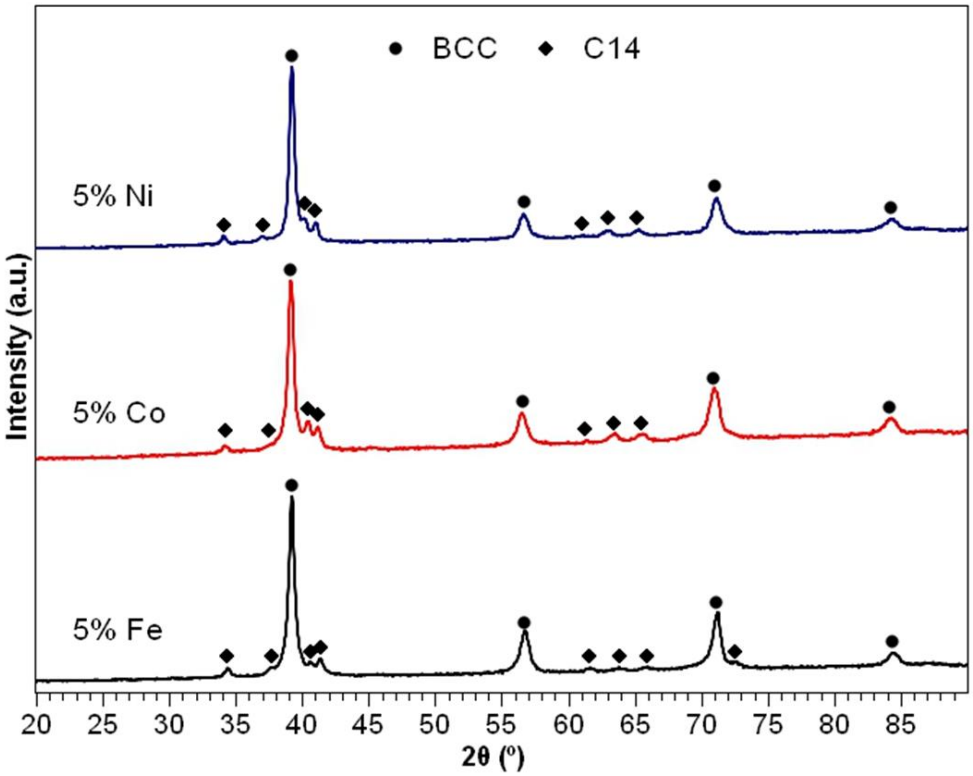

Figure 1: XRD patterns of the as-cast samples from $Ti_{31}V_{26}Nb_{26}Zr_{12}M_5$ (M=Fe, Co or Ni) alloys.

Table 2: Phase concentrations and lattice parameters determined by Rietveld refinement analyses of the as-cast, partially hydrogenated, fully hydrogenated and desorbed samples from $Ti_{31}V_{26}Nb_{26}Zr_{12}M_5$ alloys. Data values of the $Ti_{0.325}V_{0.275}Nb_{0.275}Zr_{0.125}$ alloy obtained by XRD analyses in [29,36] are given for reference as Ø.

Sample	M	a_{BCC} (Å)	%BCC	a_{FCC} (Å)	FCC (%)	a_{C14} (Å)	c_{C14} (Å)	%C14
As-cast	Ø	3.261(1)	100	--------	--------	--------	--------	--------
	Fe	3.240(1)	91	--------	--------	5.202(1)	8.408(1)	9
	Co	3.252(1)	86	--------	--------	5.239(1)	8.462(1)	14
	Ni	3.247(1)	86	--------	--------	5.254(1)	8.605(1)	14
Partially Hydrogenated 1-1.25 H/M	Ø	--------	--------	--------	--------	--------	--------	--------
	Fe	3.374(1)	69	4.475(1)	22	5.473(1)	8.933(1)	9
	Co	3.372(1)	80	4.467(1)	8	5.440(1)	8.884(1)	12
	Ni	3.370(1)	74	4.460(1)	12	5.491(1)	8.963(1)	14
Fully Hydrogenated 1.9 H/M	Ø	--------	--------	4.493(1)	100	--------	--------	--------
	Fe	--------	--------	4.472(1)	89	5.532(1)	9.025(1)	11
	Co	--------	--------	4.467(1)	87	5.537(1)	9.021(1)	13

	Ni	--------	--------	4.465(1)	87	5.584(1)	9.061(1)	13
Desorbed	Ø	3.253(1)	100	--------	--------	--------	--------	--------
	Fe	3.242(1)	89	--------	--------	5.206(1)	8.428(1)	11
	Co	3.241(1)	86	--------	--------	5.218(1)	8.474(1)	14
	Ni	3.233(1)	87	--------	--------	5.241(1)	8.613(1)	13

Figures 2 (a)-(f) display the microstructure of the as-cast alloys with Fe, Co and Ni. The three alloys presented dendritic microstructure morphology as usually reported for multicomponent alloys produced by arc melting [16,31]. Given the phase fractions observed on XRD analyses, we can infer that the BCC phases crystalized as dendrites and the C14 Laves phases crystalized at the interdendritic regions of the three alloys. The chemical composition of the different microstructural regions in the alloys were evaluated by EDS analyses as indicated in Figure 2 (b), (d) and (f). Table 3 shows the evaluated compositions of the dendritic and interdendritic regions of the alloys. It can be noticed that the alloys had pronounced segregation of Zr, Fe, Co and Ni leading to interdendritic regions richer in these elements. Exceptionally for the Co-containing alloy, the spectrum 2 (see Table 3) suggests a substantial amount of Ti segregated to the interdendritic region. However, EDS mapping (Figure 3) shows that the chemical composition in the interdendritic region of this alloy is actually Zr- and Co-rich, indicating pronounced segregation levels of only these two elements. Additional analyses of the chemical compositional gradient in the microstructure of the as cast $Ti_{31}V_{26}Nb_{26}Zr_{12}Fe_5$ and $Ti_{31}V_{26}Nb_{26}Zr_{12}Ni_5$ alloys are available in Figure S2 of the supplementary file.

Table 3: Chemical composition in at.% of as-cast alloys obtained from the dendritic and interdendritic regions. The regions analyzed via EDS are indicated in Figure 2 by red numbers.

Alloy	**Region**	**Spectrum**	**Ti**	**V**	**Nb**	**Zr**	**Fe**	**Co**	**Ni**
$Ti_{31}V_{26}Nb_{26}Zr_{12}Fe_5$	Dendritic	1	32.5	24.1	34.1	6.8	2.5	----	----
	Interdendritic	2	25.5	23.9	10.6	24	16	----	----
$Ti_{31}V_{26}Nb_{26}Zr_{12}Co_5$	Dendritic	1	30.9	26.2	33.2	8	----	1.7	----
	Interdendritic	2	44.4	9.2	8.9	30.3	----	7.2	----
$Ti_{31}V_{26}Nb_{26}Zr_{12}Ni_5$	Dendritic	1	33.5	28.1	29	8.1	----	----	1.3
	Interdendritic	2	30.4	15.1	8.3	27.5	----	----	18.7

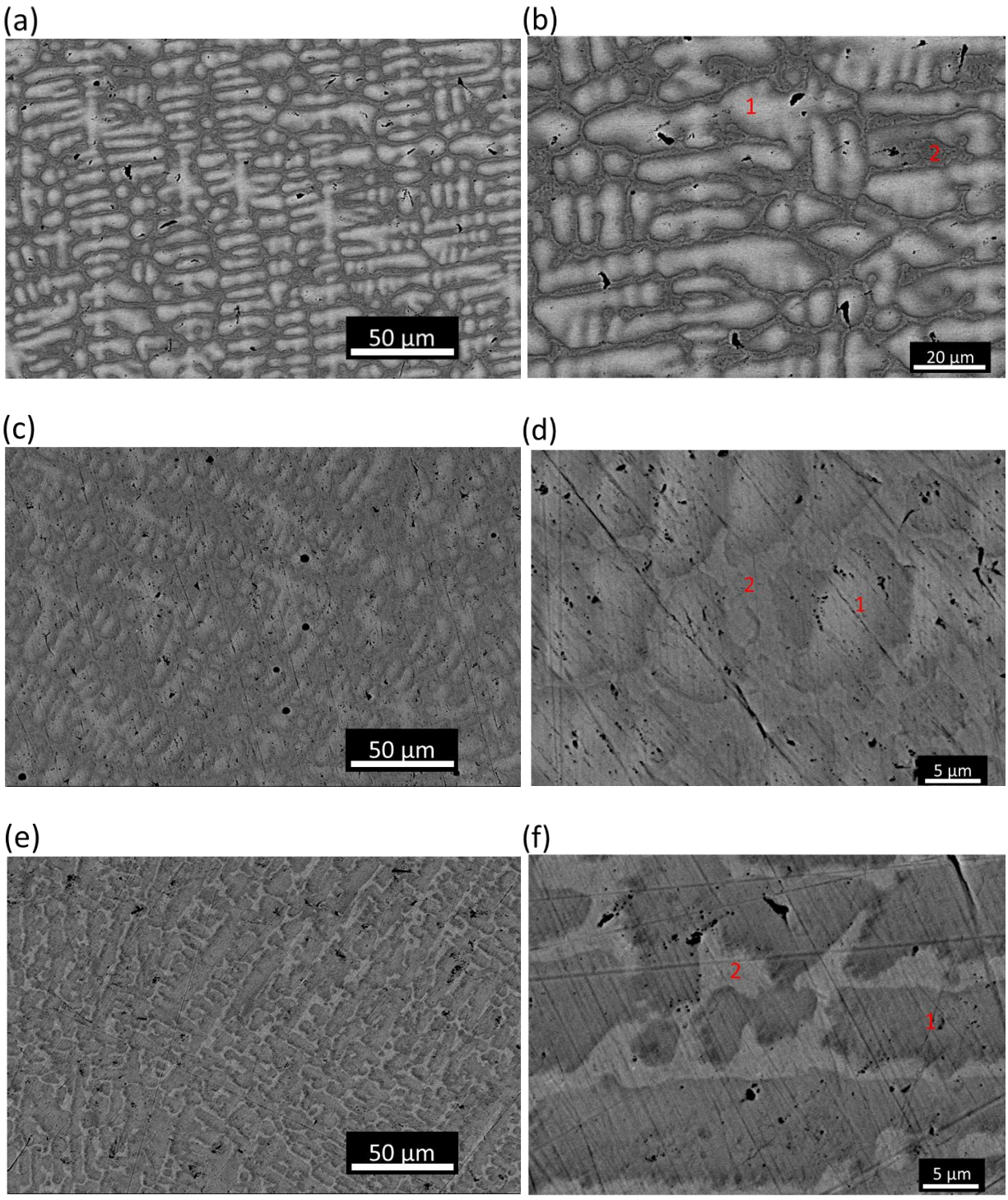

Figure 2: Back Scattered Electron (BSE) images of the microstructure of the as cast $Ti_{31}V_{26}Nb_{26}Zr_{12}M_5$ alloys with low and high magnification (a),(b) M=Fe (c),(d) M=Co (e),(f) M=Ni. Red numbers indicate the regions analyzed via EDS to evaluate the chemical composition of the dendritic and interdendritic regions.

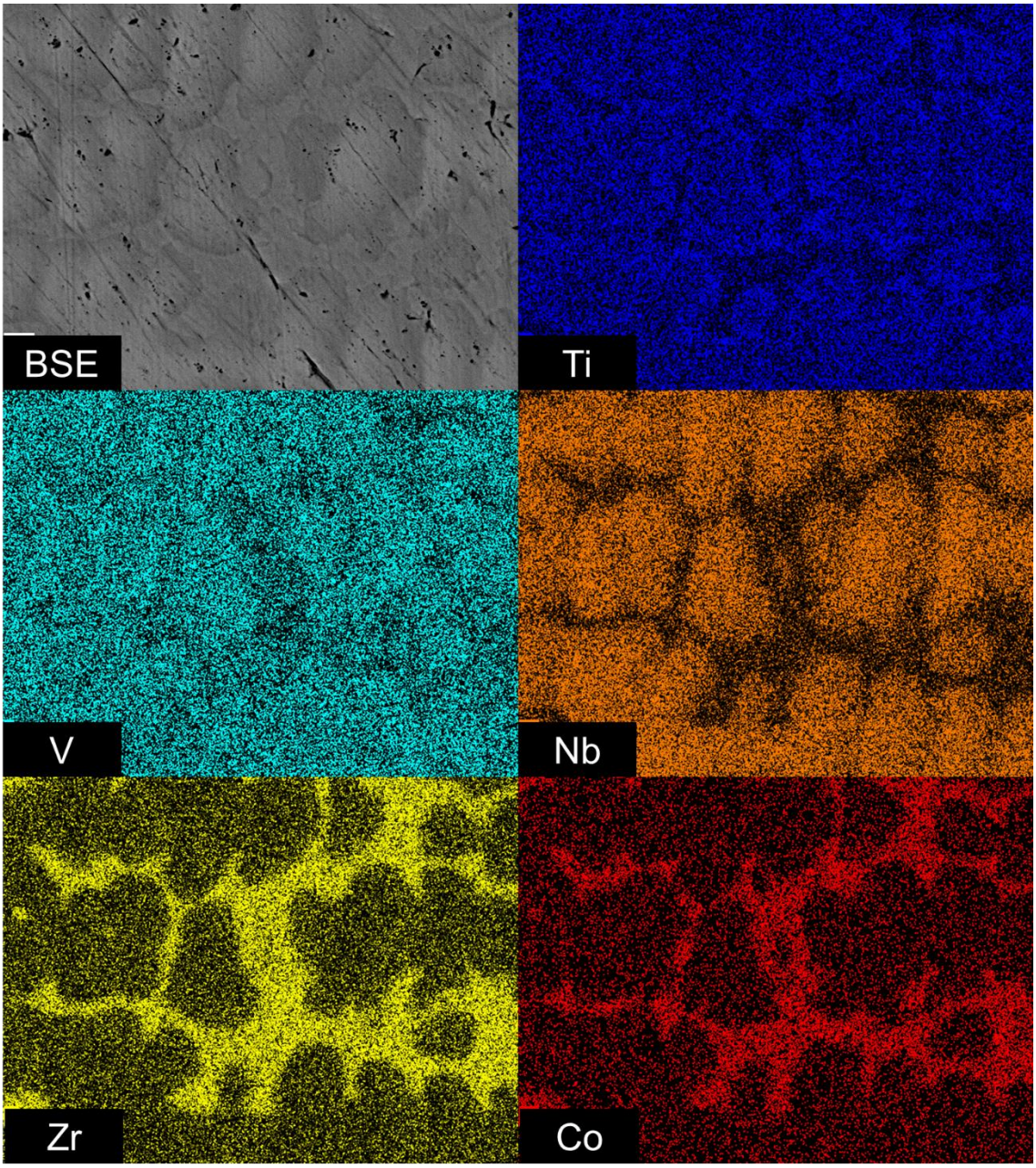

Figure 3: EDS mapping of the as-cast $Ti_{31}V_{26}Nb_{26}Zr_{12}Co_5$ alloy.

3.2. Hydrogen sorption analyses

Figure 4 (a) shows the hydrogen absorption kinetic measurements at room temperature of the $Ti_{31}V_{26}Nb_{26}Zr_{12}M_5$ alloys. The three alloys absorbed similar hydrogen content (~1.9 H/M) with fast absorption rates completing the hydrogenation process in less than one minute. This absorption level is even slightly higher than the one reported for the $Ti_{0.325}V_{0.275}Nb_{0.275}Zr_{0.125}$ base alloy (1.7-

1.8 H/M) [29,36]. It is worth noting that the Fe- containing alloy presented a slightly slower kinetics of absorption in comparison to the other alloys due to a short incubation time. This effect has been observed in other multicomponent alloys [16,18] and it is possibly associated to the effectiveness of the activation treatment for each alloy. XRD analyses were performed in the hydrogenated samples to understand the structural changes after complete absorption. Figure 4 (b) displays the XRD patterns of these samples. Lattice parameters and phase fractions determined by Rietveld refinement analyses are listed in Table 2. Rietveld refinement plots are available in Figure S3 of the supplementary file. The three fully hydrogenated samples presented multi-phase structures predominantly composed of FCC hydrides with minor amounts of C14 Laves phases. Nevertheless, upon hydrogenation the BCC phases were converted in the FCC hydrides whereas the C14 Laves phases remained with the same structure type. The hydrogenated samples with Fe, Co and Ni presented FCC hydrides with smaller lattice parameters than the FCC hydride of the $Ti_{0.325}V_{0.275}Nb_{0.275}Zr_{0.125}$ alloy. These differences in lattice parameters are similar to the ones observed for the BCC phases of the as-cast samples as earlier discussed. Another feature to be noticed is the increased lattice parameters of the C14 Laves phases in the hydrogenated samples in comparison to the as-cast samples. This feature shows that the Laves phases also absorbed hydrogen. Considering the usual uptake reported in FCC and C14 hydrides (2 H/M and 1 H/M, respectively) and the phase concentrations determined by Rietveld refinements (~12% C14 and ~88% FCC), one can see that the measurements of hydrogen absorption of our experiments (~1.9 H/M) are quite consistent. It is also important to mention that the multi-phase BCC+C14 alloys were converted in FCC+C14 hydride structures instead of BCC+C14 as reported by Sleiman et al [32]. These differences may strongly affect the maximum amount of hydrogen storage in multicomponent alloys. Moreover, the hydrogenated samples of the $Ti_{31}V_{26}Nb_{26}Zr_{12}M_5$ alloys were also characterized via SEM analyses as exhibited in Figure S4. The hydrogenation process produced refined powders due to decrepitation. This effect is well know in metal hydrides and it is associated to the high volumetric lattice expansion, strain concentration and defects generated upon hydrogen absorption [9,39,40].

(a)

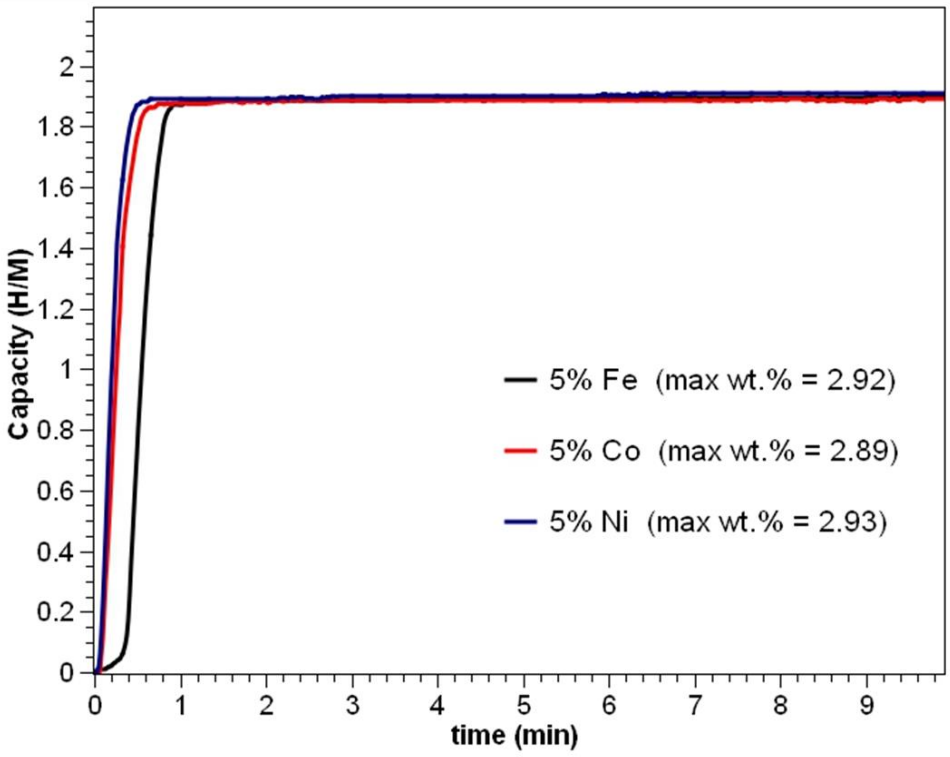
Capacity (H/M)
time (min)
5% Fe (max wt.% = 2.92)
5% Co (max wt.% = 2.89)
5% Ni (max wt.% = 2.93)

(b)

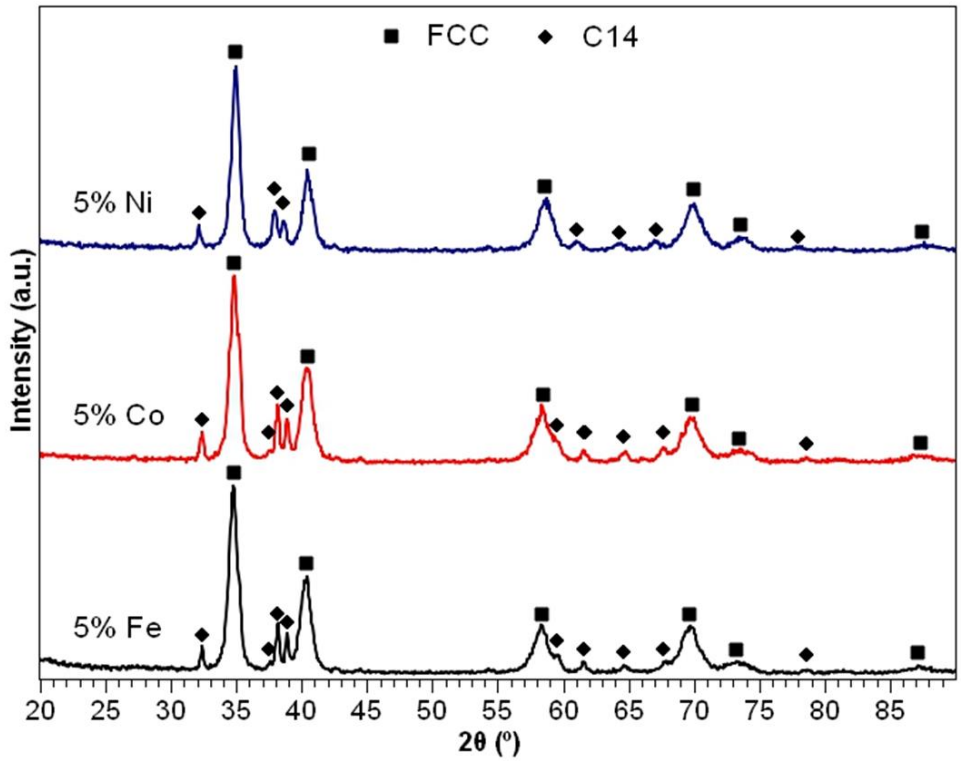
FCC
C14
5% Ni
5% Co
5% Fe
Intensity (a.u.)
2θ (°)

Figure 4: (a) Measurements of hydrogen absorption kinetics at room temperature of the $Ti_{31}V_{26}Nb_{26}Zr_{12}M_5$ alloys (b) XRD patterns of the fully hydrogenated samples after kinetic measurements.

In order to evaluate the desorption behavior of the obtained hydrides, TDS measurements were performed in the hydrogenated samples of $Ti_{31}V_{26}Nb_{26}Zr_{12}M_5$ alloys and compared with the TDS curve of $Ti_{0.325}V_{0.275}Nb_{0.275}Zr_{0.125}H_x$ reported by Montero et al. [29]. Figure 5 (a) shows the TDS curves indicating the onset temperature for hydrogen desorption in each hydrogenated sample. The samples with Fe, Co and Ni presented significantly lower on-set temperatures than the hydrogenated base alloy and other hydrogenated BCC multicomponent alloys [13,16,28,29,36]. The Fe-, Co- and Ni- containing samples also presented a more extended range of desorption temperatures than the hydrogenated base alloy. The presence of the C14 phase and the addition of non-forming hydride elements might have caused these effects on the desorption behavior of $Ti_{31}V_{26}Nb_{26}Zr_{12}M_5H_x$ samples. The high concentration of non-forming hydride elements in the C14 phases might have generated unstable C14 hydrides. In addition to this, the presence of such unstable phases might have helped to destabilize the FCC hydrides. It is also important to notice that the Fe-, Co- and Ni-containing alloys presented multi-step desorption processes. Considering this, we investigated the structure of partially hydrogenated samples of the $Ti_{31}V_{26}Nb_{26}Zr_{12}M_5$ alloys (1-1.25 H/M) to verify possible intermediate reactions of absorption/desorption. Figure 5 (b) displays the XRD patterns and the amount of hydrogen absorbed in the partially hydrogenated samples. Lattice parameters and phase fractions determined by Rietveld refinement analyses are listed in Table 2. Rietveld refinement plots are available in Figure S5 of the supplementary file. The patterns clearly show the predominant presence of BCC phases and minor amounts of FCC and C14 phases in the three samples. One can see that the lattice parameters of the BCC phases in the partially hydrogenated samples are substantially higher in comparison to the respective lattice parameters of the BCC phases in the as-cast samples. This is related to the formation of intermediate BCC monohydrides in these alloys. Considering this, we suggest that the hydrogenation process in the $Ti_{31}V_{26}Nb_{26}Zr_{12}M_5$ alloys follows reactions such as: BCC + C14 alloy ↔ intermediate BCC monohydride + C14 hydride ↔ FCC + C14 hydrides. Several BCC alloys have been reported/suggested to present intermediate hydrides during hydrogen absorption/desorption [14,16,18,25,27,31,41]. The majority of these works have shown that the intermediate hydrides absorb up to 1 H/M and at higher levels of absorption the formation of FCC

hydrides are reported with usual capacity of ~ 2 H/M. Silva et al. [41] have recently shown evidence of a miscibility gap in the BCC phase of the $(TiVNb)_{85}Cr_{15}$ multicomponent alloy that lead to the formation of an intermediate BCC hydride. We believe a similar transformation happens in the BCC phase of the $Ti_{31}V_{26}Nb_{26}Zr_{12}M_5$ alloys. Considering the FCC, BCC and C14 phase concentrations in the partially hydrogenated samples (Table 2) and the usual levels of absorption reported for these hydrides (FCC – 2 H/M), (BCC – 1 H/M) and (C14 – 1 H/M), the amount of hydrogen absorption determined in our experiments (1.22, 1.05 and 1.15 H/M) are quite consistent. Therefore, we believe the large multi-peaks desorption profile observed in the TDS curves for the $Ti_{31}V_{26}Nb_{26}Zr_{12}M_5H_x$ samples could be explained by simultaneous desorption processes of the FCC and/or C14 and/or intermediate BCC hydrides. Moreover, it is worth mentioning that the BCC+C14 multi-phase structure reported by Sleiman et al. [32] after hydrogenation of the $Ti_{0.3}V_{0.3}Mn_{0.2}Fe_{0.1}Ni_{0.1}$ alloy might be a result of incomplete reactions of absorption since the BCC phase have not generated a FCC dihydride.

Lastly, we analyzed the structure of the desorbed samples by XRD analyses. The XRD patterns are displayed in Figure 5 (c). Lattice parameters and phase fractions determined by Rietveld refinement analyses are listed in Table 2. Rietveld refinement plots are found in Figure S6 of the supplementary file. Once again, multi-phase structures were identified in the three desorbed samples. The initial BCC and C14 Laves phases were restored with similar phase fractions and lattice parameters of the as-cast samples. This confirms that indeed both phases absorbed/desorbed hydrogen and suggests that the hydrogenation process of these multicomponent alloys is reversible. Absorption/desorption cycling properties should be investigated to confirm this hypothesis. However, these evaluations are beyond the scope of this work.

(a)

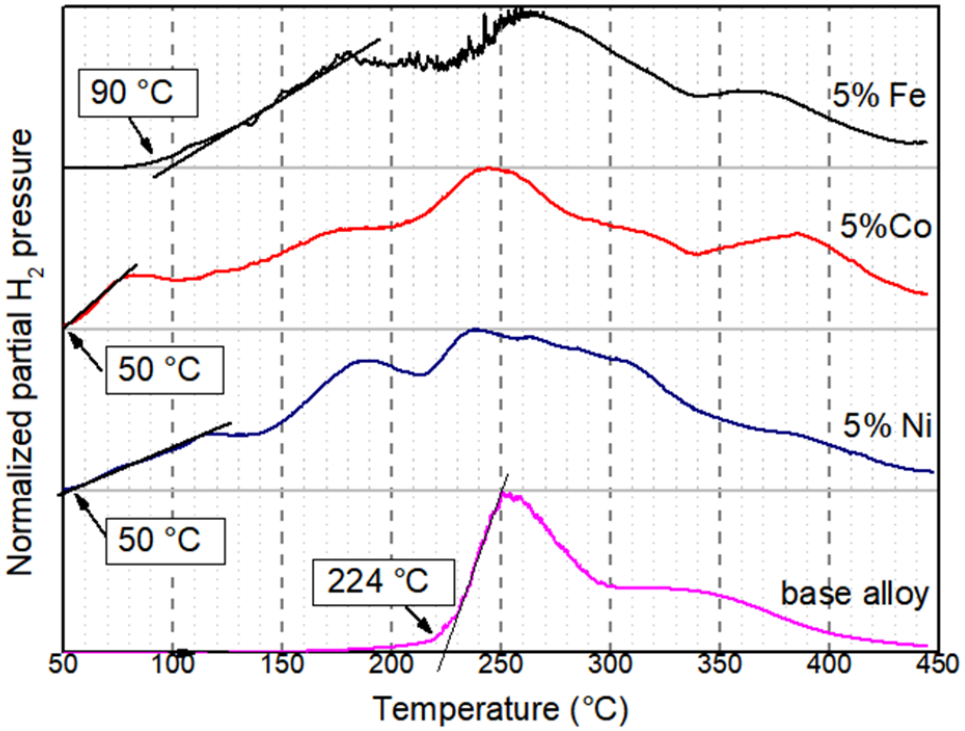
90 °C
5% Fe
5%Co
50 °C
5% Ni
50 °C
224 °C
base alloy
Normalized partial H2 pressure
50
100
150
200
250
300
350
400
450
Temperature (°C)

(b)

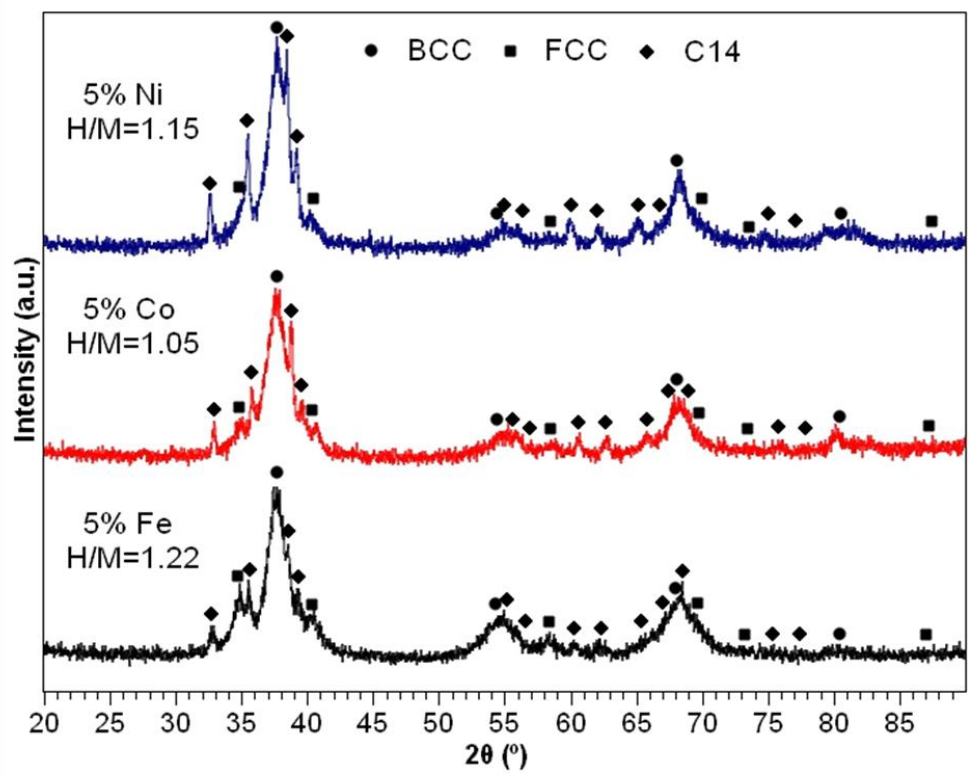
BCC
FCC
C14
5% Ni
H/M=1.15
5% Co
H/M=1.05
5% Fe
H/M=1.22
Intensity (a.u.)
20
25
30
35
40
45
50
55
60
65
70
75
80
85
2θ (º)

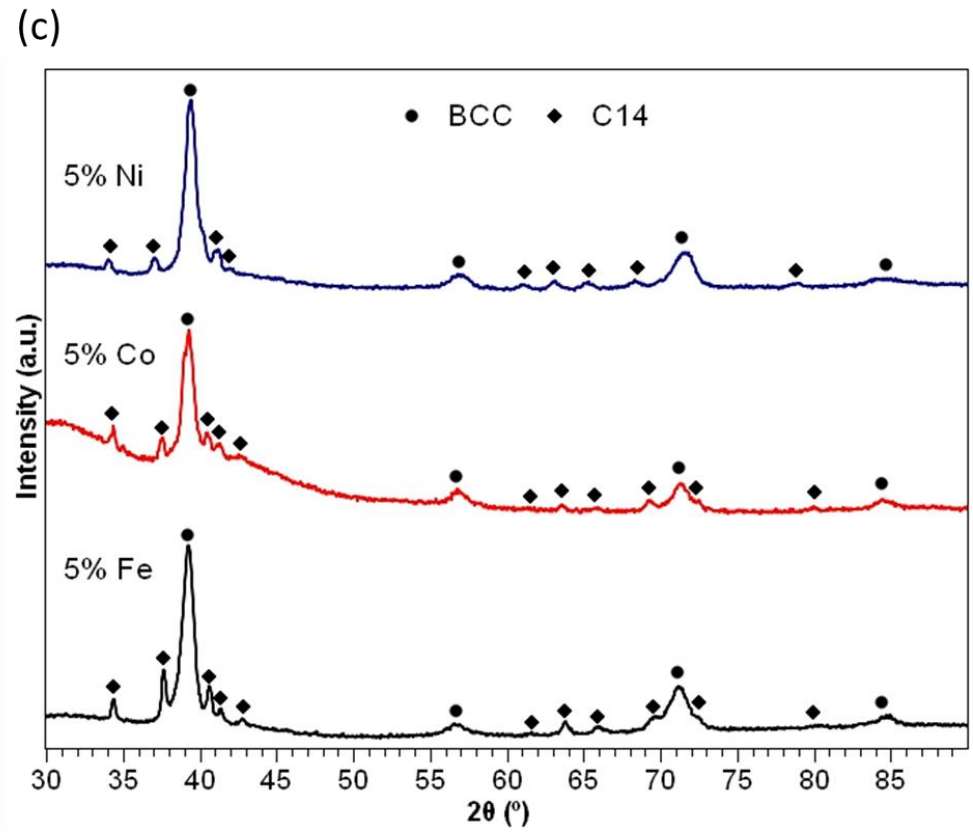

Figure 5: (a) TDS analyses of hydrogenated samples from $Ti_{31}V_{26}Nb_{26}Zr_{12}M_5$ alloys (b) XRD patterns of the partially hydrogenated samples (c) XRD patterns of the desorbed samples – desorption was conducted up to 450 ºC under secondary vacuum.

The results obtained in this work shows that multi-phase multicomponent alloys have potential to optimize storage properties via chemical compositional tuning and/or microstructural design. The three synthesized alloys successfully absorbed 1.9 H/M with fast kinetic behavior and presented an improved desorption behavior in comparison to the base alloy. Therefore, the strategy of adding non-forming hydride elements in multicomponent alloys seems promising for these multi-phase alloys. The insights of possible destabilization of FCC dihydrides via the formation of C14 hydrides might be helpful to open a pathway in the development of multi-phase multicomponent alloys for hydrogen storage. Moreover, it was shown that the reactions of hydrogen absorption/desorption of the $Ti_{31}V_{26}Nb_{26}Zr_{12}M_5$ alloys are: BCC + C14 alloy ↔ intermediate BCC hydride + C14 hydride ↔ FCC + C14 hydrides.

4. Conclusions

Three multi-phase $Ti_{31}V_{26}Nb_{26}Zr_{12}M_5$ alloys with M=Fe, Co and Ni were successfully synthesized by electric arc melting. The alloys presented dendritic microstructures composed majorly of BCC phases with small amounts of C14 phases. Each alloy absorbed approximately 1.9 H/M at room temperature with fast kinetics rate forming FCC+C14 hydrides. TDS analyses showed that the addition of non-forming hydride elements improved the desorption behavior in these alloys reducing significantly the on-set temperature for hydrogen desorption in comparison to the $Ti_{0.325}V_{0.275}Nb_{0.275}Zr_{0.125}$ alloy. Partially hydrogenated samples of $Ti_{31}V_{26}Nb_{26}Zr_{12}M_5$ alloys also indicated the presence of intermediate BCC hydrides prior to the formation of the FCC hydrides. Moreover, the desorbed samples presented similar structure to the as-cast alloys suggesting that the hydrogenation process is reversible in these alloys.

Acknowledgments

This work was financed in part by the Serrapilheira Institute (grant number Serra-1709-17362), in part by the Conselho Nacional de Desenvolvimento Científico e Tecnológico - CNPq (Project number: 142446/2019-0), in part by the CAPES-COFECUB cooperation program (process numbers 88887.387430/2019-00; 88887.314416/2019-00, project number 88887.191910/2018-00) and in part by the grant 2020/07707-6, São Paulo Research Foundation (FAPESP). This study was financed in part by the Coordenação de Aperfeiçoamento de Pessoal de Nível Superior - Brasil (CAPES) - Finance Code 001.

Data availability statement

The data used in this manuscript is available for reproduction upon request.

References

[1] IEA, Net Zero by 2050: A Roadmap for the Global Energy Sector, Int. Energy Agency. (2021) 224.

[2] S. Banerjee, M.N. Musa, A.B. Jaafar, Economic assessment and prospect of hydrogen generated by OTEC as future fuel, Int. J. Hydrogen Energy. 42 (2017) 26–37. doi:10.1016/j.ijhydene.2016.11.115.

[3] A. Züttel, A. Remhof, A. Borgschulte, O. Friedrichs, Hydrogen: The future energy carrier, Philos. Trans. R. Soc. A Math. Phys. Eng. Sci. 368 (2010) 3329–3342. doi:10.1098/rsta.2010.0113.

[4] A. Züttel, Hydrogen storage methods, Naturwissenschaften. 91 (2004) 157–172. doi:10.1007/s00114-004-0516-x.

[5] M. Dornheim, Thermodynamics of Metal Hydrides: Tailoring Reaction Enthalpies of Hydrogen Storage Materials, Thermodyn. - Interact. Stud. - Solids, Liq. Gases. (2011). doi:10.5772/21662.

[6] F. Yang, J. Wang, Y. Zhang, Z. Wu, Z. Zhang, F. Zhao, J. Huot, J. Grobivć Novaković, N. Novaković, Recent progress on the development of high entropy alloys (HEAs) for solid hydrogen storage: A review, Int. J. Hydrogen Energy. 47 (2022) 11236–11249. doi:10.1016/j.ijhydene.2022.01.141.

[7] O. Faye, J. Szpunar, U. Eduok, A critical review on the current technologies for the generation, storage, and transportation of hydrogen, Int. J. Hydrogen Energy. 47 (2022) 13771–13802. doi:10.1016/j.ijhydene.2022.02.112.

[8] N.A.A. Rusman, M. Dahari, A review on the current progress of metal hydrides material for solid-state hydrogen storage applications, Int. J. Hydrogen Energy. 41 (2016) 12108–12126. doi:10.1016/j.ijhydene.2016.05.244.

[9] Q. Lai, Y. Sun, T. Wang, P. Modi, C. Cazorla, U.B. Demirci, J.R. Ares Fernandez, F. Leardini, K.F. Aguey-Zinsou, How to Design Hydrogen Storage Materials? Fundamentals, Synthesis, and Storage Tanks, Adv. Sustain. Syst. 3 (2019) 1–64. doi:10.1002/adsu.201900043.

[10] G. Sandrock, Panoramic overview of hydrogen storage alloys from a gas reaction point of view, J. Alloys Compd. 293 (1999) 877–888. doi:10.1016/S0925-8388(99)00384-9.

[11] F. Marques, M. Balcerzak, F. Winkelmann, G. Zepon, M. Felderhoff, Review and outlook on high-entropy alloys for hydrogen storage, Energy Environ. Sci. (2021). doi:10.1039/d1ee01543e.

[12] R. Floriano, G. Zepon, K. Edalati, G.L.B.G. Fontana, A. Mohammadi, Z. Ma, H.W. Li,

R.J. Contieri, Hydrogen storage in TiZrNbFeNi high entropy alloys, designed by thermodynamic calculations, Int. J. Hydrogen Energy. 45 (2020) 33759–33770. doi:10.1016/j.ijhydene.2020.09.047.

[13] J. Montero, G. Ek, L. Laversenne, V. Nassif, G. Zepon, M. Sahlberg, C. Zlotea, Hydrogen storage properties of the refractory Ti–V–Zr–Nb–Ta multi-principal element alloy, J. Alloys Compd. 835 (2020) 155376. doi:10.1016/j.jallcom.2020.155376.

[14] C. Zlotea, M.A. Sow, G. Ek, J.P. Couzinié, L. Perrière, I. Guillot, J. Bourgon, K.T. Møller, T.R. Jensen, E. Akiba, M. Sahlberg, Hydrogen sorption in TiZrNbHfTa high entropy alloy, J. Alloys Compd. 775 (2019) 667–674. doi:10.1016/j.jallcom.2018.10.108.

[15] Y.F. Kao, S.K. Chen, J.H. Sheu, J.T. Lin, W.E. Lin, J.W. Yeh, S.J. Lin, T.H. Liou, C.W. Wang, Hydrogen storage properties of multi-principal-component CoFeMnTi xVyZrz alloys, Int. J. Hydrogen Energy. 35 (2010) 9046–9059. doi:10.1016/j.ijhydene.2010.06.012.

[16] B.H. Silva, C. Zlotea, Y. Champion, W.J. Botta, G. Zepon, Design of TiVNb-(Cr, Ni or Co) multicomponent alloys with the same valence electron concentration for hydrogen storage, J. Alloys Compd. 865 (2021) 158767. doi:10.1016/j.jallcom.2021.158767.

[17] M.M. Nygård, W.A. Sławiński, G. Ek, M.H. Sørby, M. Sahlberg, D.A. Keen, B.C. Hauback, Local order in high-entropy alloys and associated deuterides – a total scattering and Reverse Monte Carlo study, Acta Mater. 199 (2020) 504–513. doi:10.1016/j.actamat.2020.08.045.

[18] R.B. Strozi, D.R. Leiva, G. Zepon, W.J. Botta, J. Huot, Effects of the chromium content in (Tivnb)100−xcrx body-centered cubic high entropy alloys designed for hydrogen storage applications, Energies. 14 (2021). doi:10.3390/en14113068.

[19] G. Zepon, B.H. Silva, C. Zlotea, W.J. Botta, Y. Champion, Thermodynamic modelling of hydrogen-multicomponent alloy systems: Calculating pressure-composition-temperature diagrams, Acta Mater. 215 (2021) 117070. doi:10.1016/j.actamat.2021.117070.

[20] G. Zepon, D.R. Leiva, R.B. Strozi, A. Bedoch, S.J.A. Figueroa, T.T. Ishikawa, W.J. Botta, Hydrogen-induced phase transition of MgZrTiFe0.5Co0.5Ni0.5 high entropy alloy, Int. J.

Hydrogen Energy. 43 (2018) 1702–1708. doi:10.1016/j.ijhydene.2017.11.106.

[21] R.B. Strozi, D.R. Leiva, J. Huot, W.J. Botta, G. Zepon, An approach to design single BCC Mg-containing high entropy alloys for hydrogen storage applications, Int. J. Hydrogen Energy. 46 (2021) 25555–25561. doi:10.1016/j.ijhydene.2021.05.087.

[22] J. Liu, J. Xu, S. Sleiman, X. Chen, S. Zhu, H. Cheng, J. Huot, Microstructure and hydrogen storage properties of Ti–V–Cr based BCC-type high entropy alloys, Int. J. Hydrogen Energy. 46 (2021) 28709–28718. doi:10.1016/j.ijhydene.2021.06.137.

[23] P. Edalati, R. Floriano, A. Mohammadi, Y. Li, G. Zepon, H.W. Li, K. Edalati, Reversible room temperature hydrogen storage in high-entropy alloy TiZrCrMnFeNi, Scr. Mater. 178 (2020) 387–390. doi:10.1016/j.scriptamat.2019.12.009.

[24] M.M. Nygård, G. Ek, D. Karlsson, M. Sahlberg, M.H. Sørby, B.C. Hauback, Hydrogen storage in high-entropy alloys with varying degree of local lattice strain, Int. J. Hydrogen Energy. 44 (2019) 29140–29149. doi:10.1016/j.ijhydene.2019.03.223.

[25] K. Sakaki, H. Kim, K. Asano, Y. Nakamura, Hydrogen storage properties of Nb-based solid solution alloys with a BCC structure, J. Alloys Compd. 820 (2020) 153399. doi:10.1016/j.jallcom.2019.153399.

[26] M. Sahlberg, D. Karlsson, C. Zlotea, U. Jansson, Superior hydrogen storage in high entropy alloys, Sci. Rep. 6 (2016) 1–6. doi:10.1038/srep36770.

[27] M.M. Nygård, Ø.S. Fjellvåg, M.H. Sørby, K. Sakaki, K. Ikeda, J. Armstrong, P. Vajeeston, W.A. Sławiński, H. Kim, A. Machida, Y. Nakamura, B.C. Hauback, The average and local structure of TiVCrNbDx (x=0,2.2,8) from total scattering and neutron spectroscopy, Acta Mater. 205 (2021). doi:10.1016/j.actamat.2020.116496.

[28] J. Montero, G. Ek, M. Sahlberg, C. Zlotea, Improving the hydrogen cycling properties by Mg addition in Ti-V-Zr-Nb refractory high entropy alloy, Scr. Mater. 194 (2021) 113699. doi:10.1016/j.scriptamat.2020.113699.

[29] J. Montero, C. Zlotea, G. Ek, J. Crivello, L. Laversenne, M. Sahlberg, TiVZrNb Multi-Principal-Element Alloy : Sorption Properties, Molecules. 24 (2019) 1–14.

[30] D. Karlsson, G. Ek, J. Cedervall, C. Zlotea, K.T. Møller, T.C. Hansen, J. Bednarčík, M. Paskevicius, M.H. Sørby, T.R. Jensen, U. Jansson, M. Sahlberg, Structure and Hydrogenation Properties of a HfNbTiVZr High-Entropy Alloy, Inorg. Chem. 57 (2018) 2103–2110. doi:10.1021/acs.inorgchem.7b03004.

[31] M.M. Nygård, G. Ek, D. Karlsson, M.H. Sørby, M. Sahlberg, B.C. Hauback, Counting electrons - A new approach to tailor the hydrogen sorption properties of high-entropy alloys, Acta Mater. 175 (2019) 121–129. doi:10.1016/j.actamat.2019.06.002.

[32] S. Sleiman, M. Moussa, J. Huot, Microstructure and Hydrogen Storage Properties of the Multiphase Ti0.3V0.3Mn0.2Fe0.1Ni0.1 Alloy, Reactions. 2 (2021) 287–300. doi:10.3390/reactions2030018.

[33] H. Iba, E. Akiba, Hydrogen absorption and microstructure in BCC alloys with C14-type Laves phase, Nippon Kinzoku Gakkaishi/Journal Japan Inst. Met. 58 (1994) 1225–1232. doi:10.2320/jinstmet1952.58.10_1225.

[34] R.R. Shahi, A.K. Gupta, P. Kumari, Perspectives of high entropy alloys as hydrogen storage materials, Int. J. Hydrogen Energy. (2022). doi:10.1016/j.ijhydene.2022.02.113.

[35] R.B. Strozi, D.R. Leiva, J. Huot, W.J. Botta, G. Zepon, Synthesis and hydrogen storage behavior of Mg–V–Al–Cr–Ni high entropy alloys, Int. J. Hydrogen Energy. 46 (2021) 2351–2361. doi:10.1016/j.ijhydene.2020.10.106.

[36] J.M. Banuelos, Refractory high entropy alloys for hydrogen storage, Université Paris-Est, 2020.

[37] B.H. Toby, R.B. Von Dreele, GSAS-II: the genesis of a modern open-source all purpose crystallography software package, J. Appl. Crystallogr. 46 (2013) 544–549. doi:10.1107/S0021889813003531.

[38] J.C. Slater, Atomic radii in crystals, J. Chem. Phys. 41 (1964) 3199–3204. doi:10.1063/1.1725697.

[39] A. Züttel, Materials for hydrogen storage, Mater. Today. 6 (2003) 24–33. doi:10.1016/S1369-7021(03)00922-2.

[40] H.C. Lin, K.M. Lin, K.C. Wu, H.H. Hsiung, H.K. Tsai, Cyclic hydrogen absorption-desorption characteristics of TiCrV and Ti0.8 Cr1.2 V alloys, Int. J. Hydrogen Energy. 32 (2007) 4966–4972. doi:10.1016/j.ijhydene.2007.07.057.

[41] B.H. Silva, C. Zlotea, G. Vaughan, Y. Champion, W.J. Botta, G. Zepon, Hydrogen absorption/desorption reactions of the (TiVNb)85Cr15 multicomponent alloy, J. Alloys Compd. 901 (2022) 163620. doi:10.1016/j.jallcom.2022.163620.